Novel Pd_{2}Se_{3} Two-Dimensional Phase Driven by Interlayer Fusion in Layered PdSe_{2}

Junhao Lin, Sebastian Zuluaga, Peng Yu, Zheng Liu, Sokrates T. Pantelides, and Kazu Suenaga

Phys. Rev. Lett. **119**, 016101 — Published 6 July 2017

DOI: 10.1103/PhysRevLett.119.016101

A novel Pd_2Se_3 two-dimensional phase driven by interlayer fusion in layered $PdSe_2$

Junhao Lin[1*], Sebastian Zuluaga[2], Peng Yu[3], Zheng Liu[3,4,5], Sokrates T. Pantelides[2,6], and Kazu Suenaga[1,7*]

[1] National Institute of Advanced Industrial Science and Technology (AIST), AIST Central 5, Tsukuba 305-8565, Japan
[2] Department of Physics and Astronomy, Vanderbilt University, Nashville, TN 37235, USA
[3] Centre for Programmed Materials, School of Materials Science and Engineering, Nanyang Technological University, Singapore 639798, Singapore
[4] NOVITAS, Nanoelectronics Centre of Excellence, School of Electrical and Electronic Engineering, Nanyang Technological University, Singapore 639798, Singapore
[5] Centre for Disruptive Photonic Technologies, School of Physical and Mathematical Sciences, Nanyang Technological University, Singapore 637371, Singapore
[6] Department of Electrical Engineering and Computer Science, Vanderbilt University, Nashville, TN 37235, USA
[7] Department of Mechanical Engineering, The University of Tokyo, Tokyo 113-8656, Japan

* Correspondence and requests for materials should be addressed to: lin.junhao@aist.go.jp or suenaga-kazu@aist.go.jp

Abstract:

Two-dimensional (2D) materials are easily fabricated when their bulk form has a layered structure. The monolayer form in layered transition-metal dichalcogenides is typically the same as a single layer of the bulk material. However, $PdSe_2$ presents a puzzle. Its monolayer form has been theoretically shown to be stable, but there have been no reports that monolayer $PdSe_2$ has been fabricated. Here, combining atomic-scale imaging in a scanning transmission electron microscope and density functional theory, we demonstrate that the preferred monolayer form of this material amounts to a melding of two bulk monolayers accompanied by the emission of Se atoms so that the resulting stoichiometry is Pd_2Se_3. We further verify the interlayer melding mechanism

by creating Se vacancies *in situ* in the layered $PdSe_2$ matrix using electron irradiation. The discovery that strong interlayer interactions can be induced by defects and lead to the formation of new 2D materials opens a new venue for the exploration of defect engineering and novel 2D structures.

The discovery of graphene has stimulated intense research in two-dimensional (2D) materials [1–4], due to the fascinating physical properties that are dramatically different from those of their bulk counterpart [5–8]. Noble-metal dichalcogenides have attracted significant attention recently due to their unique atomic and electronic structures [9–11]. $PdSe_2$ is one of these novel 2D noble-metal dichalcogenides known for its remarkable layer-dependent electronic structure [12–15]: monolayer $PdSe_2$ is predicted to be an indirect band gap semiconductor with a band gap of 1.43 eV, while the bulk exhibits a band gap of 0.03 eV [16]. In contrast to the frequently reported 1H and 1T (hexagonal) phases in layered transition-metal dichalcogenides (TMDs), $PdSe_2$ has an uncommon structure. Pd atoms coordinate with four Se atoms, forming a square backbone network [16–18] (Figure 1A). Whereas in most TMDs with 1H and 1T structures there is only metal-chalcogen bonding [12,14], the two Se atoms located in the top and bottom planes of the $PdSe_2$ structure form a tilted Se-Se dumbbell crossing the Pd layer, which results in the lack of rotational symmetry. Such structure is potentially sensitive against defects, as Se vacancies would break the symmetry of the Se-Se dumbbell and induce large structural distortion. This is in sharp contrast to the commonly observed 1H or 1T monolayer dichalcogenides, where the chalcogen vacancies can be accommodated at several concentrations leaving the lattice intact [19,20]. Therefore, even though bulk $PdSe_2$ has been experimentally synthesized and investigated [17,21], little is known on its monolayer form on the experimental side.

In this paper we report the successful exfoliation of a stable monolayer phase from bulk $PdSe_2$, but this phase does not have the expected $PdSe_2$ stoichiometry and atomic structure. Combining scanning transmission electron microcopy (STEM) imaging and first-principles calculations, we unambiguously determine that the new monolayer phase has a novel atomic structure and its stoichiometry is Pd_2Se_3. Furthermore, the formation of the Pd_2Se_3 monolayer has its roots in Se vacancies in the $PdSe_2$ system. Unlike most 2D layered materials such as graphene and MoS_2, whose layers interact with each other only through weak van der Waal forces, even in the presence of defects, we show that, in $PdSe_2$, Se vacancies reduce the distance between layers causing the melding of two layers into one, resulting in the formation of the new Pd_2Se_3 2D phase. This process is verified by successfully fabricating a Pd_2Se_3 monolayer using the microscope's electron beam and by observing in-situ the Pd_2Se_3-monolayer growth along the edge of the few-layer $PdSe_2$ matrix.

We used the routine scotch-tape method to exfoliate a monolayer from bulk $PdSe_2$ (schematic shown in Figure 1A). Figure 1B shows a small area that exhibits three distinct regions whose atomic structures are clearly visualized. Since the image intensity in STEM imaging is linearly proportional to the thickness of the few-layered film [22,23], the intensity profile suggests the layer-by-layer thinning from tri-layer to (quasi) monolayer (detailed discussion in Fig. S1). The monolayer region shows a very discrete atomic contrast. Furthermore, the intensity of the monolayer region shows a deviation from the expected linear trend in layered materials (Fig. S1), suggesting that the monolayer may contain more atoms than expected.

Figures 2A – 2D show experimental zoom-in images with atomic resolution (grey figures) and simulated ones (yellow figures) of the monolayer, bilayer and trilayer regions, respectively. Both the bilayer and trilayer agree well with the conventional stacking order in

layered $PdSe_2$ (Figures 2C and 2D), while the monolayer (Figure 2A), surprisingly, displays a completely different lattice structure from the monolayer $PdSe_2$ expected from the bulk (Figure 2B). In order to study this discrepancy, electron energy loss spectroscopy (EELS) was applied to examine the chemical purity of the monolayer (Fig. S1), but no apparent difference is detected when compared to the bilayer $PdSe_2$ in a wide energy region, *i.e.*, the monolayer still comprises Pd and Se atoms only. Note that the electron dose during the imaging is controlled at a moderate level so that the electrons have a negligible effect on the monolayer structure. These results indicate that the monolayer has a different atomic structure than the expected monolayer model of $PdSe_2$, *i.e.*, a spontaneous reconstruction occurs in the monolayer limit of $PdSe_2$.

A fast Fourier transformation (FFT, similar to diffractogram) of the whole high-resolution ADF STEM image (Figure 1B) shows a clear epitaxial relationship between the few layers and the monolayer region, see inset in Figure 1B. This phenomenon suggests that the monolayer was presumably reconstructed from the bilayer $PdSe_2$, and thus maintained the crystal orientation of the few-layer region. The FFT also suggests that the reconstructed monolayer inherits the squared network and unit cell parameters from the $PdSe_2$ bilayer, similar to the lateral epitaxial behavior. A careful comparison of the FFT patterns between the reconstructed monolayer and the $PdSe_2$ bilayer reveals more information about the heritage of the lattice symmetry (see the left panels in Figure 2A and 2C). Figure 2C (bilayer $PdSe_2$ region) shows a squared pattern with the principal diffraction points at the (200) plane (corresponding to ~3Å lattice periodicity), which is consistent with the bulk $PdSe_2$ model. While the left panel of Figure 2A (monolayer region) shows that the diffraction point of (110) plane (corresponding to ~ 4.2Å lattice periodicity in the bilayer $PdSe_2$ model) becomes dominant in the reconstructed monolayer region. It is clear that the unit cell of the

reconstructed monolayer maintains a different lattice symmetry, whereas it is still squared but with an expanded periodicity from 3 Å to 4.2 Å. Simulations of the diffraction patterns are consistent with the above analysis (Fig. S2). These results imply that a novel heritage process occurs during the reconstruction of the monolayer.

Combining the quantitative STEM image intensity analysis on each atomic column with density functional theory (DFT), we were able to find a novel and stable monolayer phase with a unique structure and new stoichiometry of Pd_2Se_3, that matches the experimental STEM image of the monolayer, as shown in Figure 2A. It is important to note that, to the extent of our knowledge, this structure has never been reported, even as a bulk phase. Furthermore, the new Pd_2Se_3 monolayer phase is physically stable as indicated by DFT phonon calculations and quantum molecular dynamics simulations (see detailed discussion in Figure S3) and exhibits a cohesive energy of 1.26 eV/atom, higher than the hypothetical $PdSe_2$ monolayer obtained from bulk (0.98 eV/atom). This means that the chemical bonding of the Pd_2Se_3 monolayer is more robust. In this new Pd_2Se_3 monolayer, the Se-Se dumbbell is paired with another Se atom, each of which bonds to four Pd atoms in the squared network. Furthermore, the covalent Se-Se dumbbell is now outside and parallel to the Pd layer instead of crossing it, similar to the atomic-layer configuration found in 1H or 1T phases, in which chalcogen vacancies can be accommodated without much reconstruction (Fig. S4). It is notable that, all monolayer regions are in the Pd_2Se_3 phase other than $PdSe_2$ (Fig. S5), suggesting the monolayer $PdSe_2$ phase is highly unstable in the ambient condition. The bulk Pd_2Se_3 phase is predicted to also be a van der Waals-type layered material and observed in experiment (Fig. S6), where the layers are stacked periodically with an interlayer binding energy of 50 meV, the same order of magnitude as other layered materials [24]. The Pd_2Se_3

monolayer phase is predicted to be a semiconductor with a different bandgap value from its parent material (Fig. S7).

By comparing the lattice structures, we found the similarities between the $PdSe_2$ and Pd_2Se_3 phases. As displayed in Figure 3A, square Pd backbone in the reconstructed Pd_2Se_3 monolayer phase looks very similar to bilayer $PdSe_2$. If the Pd atoms from the two $PdSe_2$ layers (red and blue dashed squares in Figure 3A) are merged vertically into the same layer but keeping their x-y coordination unchanged, a shorter Pd-Pd distance of the squared network (green dashed squares) can be obtained, which is almost identical to that in the Pd_2Se_3 monolayer (3 Å). This observation can explain the epitaxial behavior between the Pd_2Se_3 monolayer and $PdSe_2$ bilayer as shown in the FFT patterns, *i.e.*, the unit cell in both structures has a squared lattice but in different lattice symmetry. This result suggests that the reconstruction possibly involves merging of the two layers.

The chemical stoichiometry changing from $PdSe_2$ to Pd_2Se_3 suggests a Se-deficient condition in the parent materials. We performed DFT calculations on the Se vacancies in the $PdSe_2$ bilayer and found that as the concentration of Se vacancies increases, the interlayer distance decreases, as evidenced in Figure 3B. It is important to notice that the interlayer distance decreases from 4.55 Å to 2.84 Å (by 1.71 Å) when reaching the Pd_2Se_3 chemical stoichiometry, which is almost the length of a typical Pd-Se bond (2.5 Å), providing the premise for the merging of the two layers. The origin of the Se-vacancy-driven decrease in interlayer distance lies in the substantial reconstruction of the Pd atoms in the $PdSe_2$ bilayer. The undercoordinated Pd atoms try to bond with the nearest Se atom, in this case, the one in the adjacent layer, which creates quantum force that pulls two layers towards each other as predicted by calculations (detail in Fig. S8). Such feature is absent in other TMD materials

such as MoS_2, where the reconstruction of Mo atoms is protected by the crystal symmetry (Fig. 3B). Furthermore, we enquired whether Se vacancies can be passivated by ambient oxygen. We found that oxygen has a negligible effect on the vacancy-mediated interlayer melding (see Fig. S9).

The results presented above allow us to conclude that the Pd_2Se_3 reconstruction originates from an "interlayer fusion" mechanism. This mechanism is driven by Se vacancies and merges the Pd backbones from the two layers into one, which subsequently leads to the rearrangement of the Se atoms resulting in the formation of the Pd_2Se_3 monolayer, thus preserving all the lattice parameters of bilayer $PdSe_2$. This "interlayer fusion" evolution path is further supported by the DFT calculations in the energy landscape. Figure 3C illustrates the difference in total energy between the defective bilayer $PdSe_2$ with Se vacancies (Pd_2Se_3 stoichiometry) and the reconstructed monolayer Pd_2Se_3. The latter is 1.36 eV/unit cell lower in energy, suggesting the monolayer Pd_2Se_3 as the energetically preferred system. The energy barrier is ~ 0.67 eV which can be overcome by thermal or electron beam excitations.

Chalcogen deficiency in layered TMD materials can be intentionally introduced by electron irradiation and often induces massive reconstructions leading to new metastable structures [25–28]. We attempted to create Se-deficient conditions using electron irradiation in $PdSe_2$, *i.e.*, artificially providing a reconstruction condition for Pd_2Se_3 in the $PdSe_2$ matrix through interlayer fusion and simultaneously captured the *in situ* dynamical growing process. Figure 4 shows a series of snapshots of sequential STEM images of the reconstruction process from the bilayer $PdSe_2$ to monolayer Pd_2Se_3 in two cases. Figure 4A shows the growth of the Pd_2Se_3 monolayer extending into the bilayer $PdSe_2$ matrix gradually with the same lattice orientation as the electron dose increased. The growth process provides a direct evidence of

the heritage of the new monolayer via interlayer fusion. Figure 4B shows another case where the growth of monolayer Pd_2Se_3 has a misoriented angle from the parent bilayer $PdSe_2$. A small patch of Pd_2Se_3 monolayer may have rotated during the electron beam excitation, then the subsequent lattice fuses at the edge of bilayer $PdSe_2$ and realigns with the crystal orientation of its template Pd_2Se_3 monolayer. All these evidence unambiguously shows the Pd_2Se_3 monolayer can be directly created from the $PdSe_2$ matrix as found by our DFT calculations.

In conclusion, we report a novel Pd_2Se_3 monolayer phase reconstructed from few-layers of $PdSe_2$ via interlayer fusion, with all the lattice parameters and the metal network inherited virtually intact. Combining DFT calculations and in-situ dynamical observations, we further unveil that the reconstruction of Pd_2Se_3 originates from the extraordinary interlayer interaction between the $PdSe_2$ layers, as driven by the introduction of Se vacancies in pristine $PdSe_2$. Due to the inevitable Se vacancies that trigger the observed interlayer fusion, it remains uncertain whether the intrinsic monolayer $PdSe_2$ phase is experimentally achievable by the top-down exfoliation method or even a bottom-up fabrication like chemical vapor deposition (CVD), though predicted stable by our DFT calculations (Fig. S3). The monolayer materials that have been reported so far in the literature show the same crystal structure as the bulk layers without exception. This work clearly demonstrates a discrepancy occurs in atomic structure between the monolayer and bulk phase due to the strong interlayer interaction.

Acknowledgement:

J.L. and K.S. acknowledge JST-ACCEL and JSPS KAKENHI (JP16H06333 and P16823) for financial support. Work at Vanderbilt was supported by the U.S. Department of Energy via grant No. DE-FG02-09ER46554 and by the McMinn Endowment (S.Z., S.T.P.). J.L. and K.S.

conceived the idea. J.L. performed the sample preparation and STEM-EELS measurements and analyzed the data. S.Z. performed the DFT calculations with the help from J.L. and S.T.P. Y.P. and Z.L. provided the bulk sample. All authors discussed the results and their interpretations. J.L. and S.Z. co-wrote the manuscript with contributions from K.S. and S.T.P. who also supervised the project.

References:

[1] K. S. Novoselov, D. Jiang, F. Schedin, T. J. Booth, V. V Khotkevich, S. V Morozov, and a K. Geim, Proc. Natl. Acad. Sci. U. S. A. **102**, 10451 (2005).

[2] A. K. Geim and I. V Grigorieva, Nature **499**, 419 (2014).

[3] A. H. Castro Neto, F. Guinea, N. M. R. Peres, K. S. Novoselov, and A. K. Geim, Rev. Mod. Phys. **81**, 109 (2009).

[4] K. S. Novoselov, A. K. Geim, S. V Morozov, D. Jiang, Y. Zhang, S. V Dubonos, I. V Grigorieva, and A. A. Firsov, Source Sci. New Ser. Gene Expr. Genes Action **306**, 666 (2004).

[5] Y. Chen, J. Xi, D. O. Dumcenco, Z. Liu, K. Suenaga, D. Wang, Z. Shuai, Y.-S. Huang, and L. Xie, ACS Nano **7**, 4610 (2013).

[6] A. Splendiani, L. Sun, Y. Zhang, T. Li, J. Kim, C. Y. Chim, G. Galli, and F. Wang, Nano Lett. **10**, 1271 (2010).

[7] X. Xi, L. Zhao, Z. Wang, H. Berger, L. Forró, J. Shan, and K. F. Mak, Nat. Nanotechnol. **10**, 1 (2015).

[8] M. M. Ugeda, A. J. Bradley, Y. Zhang, S. Onishi, Y. Chen, W. Ruan, C. Ojeda-Aristizabal, H. Ryu, M. T. Edmonds, H.-Z. Tsai, A. Riss, S.-K. Mo, D. Lee, A. Zettl, Z. Hussain, Z.-X. Shen, and M. F. Crommie, Nat. Phys. **12**, 92 (2015).

[9] Y. Zhao, J. Qiao, Z. Yu, P. Yu, K. Xu, S. P. Lau, W. Zhou, Z. Liu, X. Wang, W. Ji, and Y. Chai, Adv. Mater. (2016).

[10] Y. Wang, L. Li, W. Yao, S. Song, J. T. Sun, J. Pan, X. Ren, C. Li, E. Okunishi, Y. Q. Wang, E. Wang, Y. Shao, Y. Y. Zhang, H. T. Yang, E. F. Schwier, H. Iwasawa, K. Shimada, M. Taniguchi, Z. Cheng, S. Zhou, S. Du, S. J. Pennycook, S. T. Pantelides, and H. J. Gao, Nano Lett. **15**, 4013 (2015).

[11] M. Ghorbani-Asl, A. Kuc, P. Mir??, and T. Heine, Adv. Mater. **28**, 853 (2016).

[12] M. Chhowalla, H. S. Shin, G. Eda, L.-J. Li, K. P. Loh, and H. Zhang, Nat Chem **5**, 263 (2013).

[13] P. Miro, M. Ghorbani-Asl, and T. Heine, Angew. Chemie - Int. Ed. **53**, 3015 (2014).

[14] Q. H. Wang, K. Kalantar-Zadeh, A. Kis, J. N. Coleman, and M. S. Strano, Nat. Nanotechnol. **7**, 699 (2012).

[15] P. Miro, M. Audiffred, and T. Heine, Chem. Soc. Rev. **43**, 6537 (2014).

[16] J. Sun, H. Shi, T. Siegrist, and D. J. Singh, Appl. Phys. Lett. **107**, 2 (2015).

[17] F. Grønvold and E. Røst, Acta Crystallogr. **10**, 329 (1957).

[18] Y. Wang, Y. Li, and Z. Chen, J. Mater. Chem. C **3**, 9603 (2015).

[19] J. Hong, Z. Hu, M. Probert, K. Li, D. Lv, X. Yang, L. Gu, N. Mao, Q. Feng, L. Xie, J. Zhang, D. Wu, Z. Zhang, C. Jin, W. Ji, X. Zhang, J. Yuan, and Z. Zhang, Nat. Commun. **6**, 6293 (2015).

[20] G. Ye, Y. Gong, J. Lin, B. Li, Y. He, S. T. Pantelides, W. Zhou, R. Vajtai, and P. M. Ajayan, Nano Lett. **16**, 1097 (2016).

[21] C. Soulard, X. Rocquefelte, P.-E. Petit, M. Evain, S. Jobic, J.-P. Itié, P. Munsch, H.-J. Koo, and M.-H. Whangbo, Inorg. Chem. **43**, 1943 (2004).

[22] X. Lu, M. I. B. Utama, J. Lin, X. Gong, J. Zhang, Y. Zhao, S. T. Pantelides, J. Wang, Z. Dong, Z. Liu, W. Zhou, and Q. Xiong, Nano Lett. **14**, 2419 (2014).

[23] W. Zhou, X. Zou, S. Najmaei, Z. Liu, Y. Shi, J. Kong, J. Lou, P. M. Ajayan, B. I. Yakobson, and J. C. Idrobo, Nano Lett **13**, 2522 (2013).

[24] T. Bjorrkman, A. Gulans, A. V. Krasheninnikov, and R. M. Nieminen, Phys. Rev. Lett. **108**, 1 (2012).

[25] J. Lin, O. Cretu, W. Zhou, K. Suenaga, D. Prasai, K. I. Bolotin, N. T. Cuong, M. Otani, S. Okada, A. R. Lupini, J.-C. Idrobo, D. Caudel, A. Burger, N. J. Ghimire, J. Yan, D. G. Mandrus, S. J. Pennycook, and S. T. Pantelides, Nat. Nanotechnol. **9**, 436 (2014).

[26] J. Lin, S. T. Pantelides, and W. Zhou, ACS Nano **9**, 5189 (2015).

[27] X. Liu, T. Xu, X. Wu, Z. Zhang, J. Yu, H. Qiu, J.-H. Hong, C.-H. Jin, J.-X. Li, X.-R. Wang, L.-T. Sun, and W. Guo, Nat. Commun. **4**, 1776 (2013).

[28] J. Lin, Y. Zhang, W. Zhou, and S. T. Pantelides, ACS Nano **10**, 2782 (2016).

[29] See Supplemental Material [url] for the preparation of the TEM sample, detailed information of the STEM characterization and DFT calculation, and supplementary Figures S1-S9, which includes Refs. [30-38].

[30] K. S. Novoselov, A. K. Geim, S. V Morozov, D. Jiang, Y. Zhang, S. V Dubonos, I. V Grigorieva, and A. A. Firsov, Science (80-.). **306**, 666 (2004).

[31] G. Kresse and J. Furthmüller, Phys. Rev. B **54**, 11169 (1996).

[32] G. Kresse, Phys. Rev. B **59**, 1758 (1999).

[33] T. Thonhauser, S. Zuluaga, C. A. Arter, K. Berland, E. Schr??der, and P. Hyldgaard, Phys. Rev. Lett. **115**, 1 (2015).

[34] K. Berland, V. R. Cooper, K. Lee, E. Schröder, T. Thonhauser, P. Hyldgaard, and B. I. Lundqvist, Reports Prog. Phys. **78**, 66501 (2015).

[35] D. C. Langreth, B. I. Lundqvist, S. D. Chakarova-Käck, V. R. Cooper, M. Dion, P. Hyldgaard, a Kelkkanen, J. Kleis, L. Kong, S. Li, P. G. Moses, E. Murray, a Puzder, H. Rydberg, E. Schröder, and T. Thonhauser, J. Phys. Condens. Matter **21**, 84203 (2009).

[36] T. Thonhauser, V. R. Cooper, S. Li, A. Puzder, P. Hyldgaard, and D. C. Langreth, Phys. Rev. B - Condens. Matter Mater. Phys. **76**, 1 (2007).

[37] K. Appavoo, B. Wang, N. F. Brady, M. Seo, J. Nag, R. P. Prasankumar, D. J. Hilton, S. T. Pantelides, and R. F. Haglund, Nano Lett. **14**, 1127 (2014).

[38] Y. Y. Zhang, R. Mishra, T. J. Pennycook, A. Y. Borisevich, S. J. Pennycook, and S. T. Pantelides, Adv. Mater. Interfaces **2**, 1500344 (2015).

FIGURES:

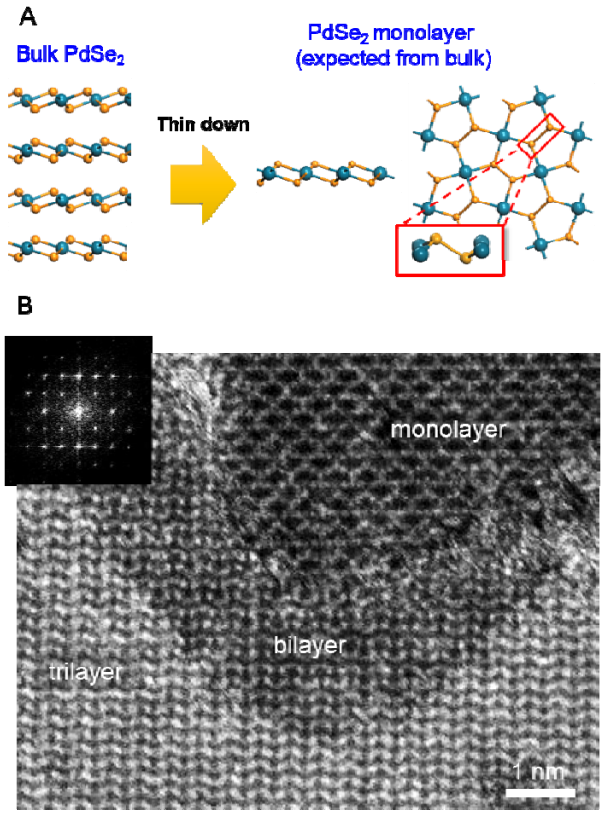

Figure 1: Exfoliation of layered $PdSe_2$ sample. (A) Schematic of the expected exfoliation of monolayer $PdSe_2$ from its bulk form. The atomic structural model is shown with the Se-Se dumbbell highlighted as the inset. (B) High resolution ADF STEM images showing a thin few-layer $PdSe_2$ region. The number of the layers can be identified by the difference of the image contrast. The inset is the FFT pattern of the whole image.

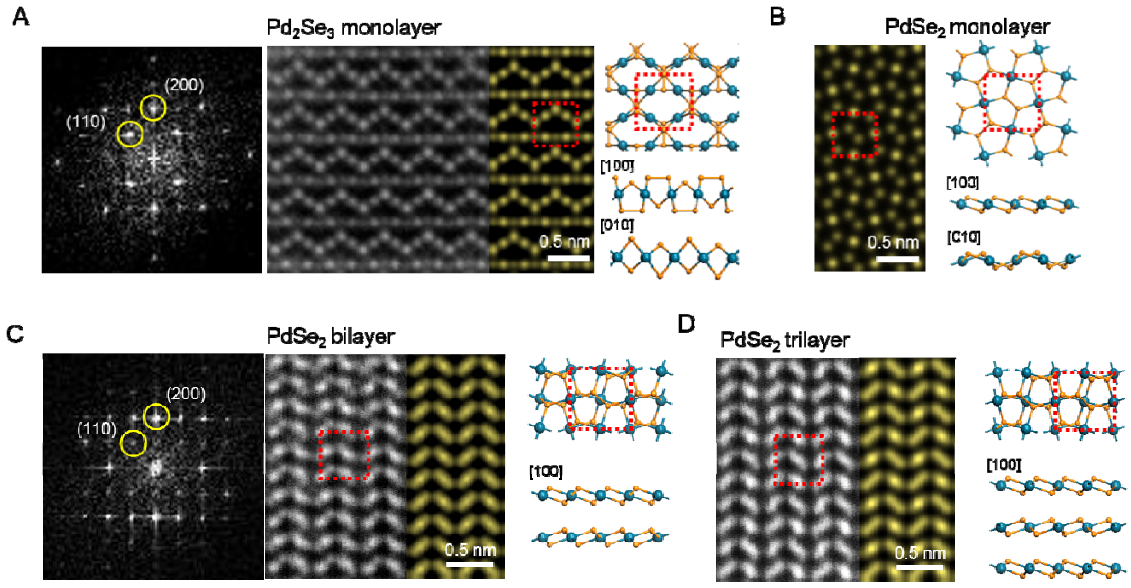

Figure 2: Atomic resolution STEM images of the reconstructed monolayer Pd_2Se_3 and few layer $PdSe_2$. (A-D) High resolution experimental (grey) and simulated (yellow) ADF STEM image of reconstructed Pd_2Se_3 monolayer (A), the hypothetical $PdSe_2$ monolayer (B, only simulated, not observed in experiment), $PdSe_2$ bilayer (C) and $PdSe_2$ trilayer (D). The Fast Fourier transformation (FFT) of the Pd_2Se_3 monolayer and $PdSe_2$ bilayer region are displayed in the left hand side of panels (A), and (C), respectively. The FFT indicates that even though the two systems have different lattice symmetry, they have similar lattice parameters. The principle diffraction planes of interest are highlighted by yellow circles. The unit cells of each structure are highlighted with red dashed squares.

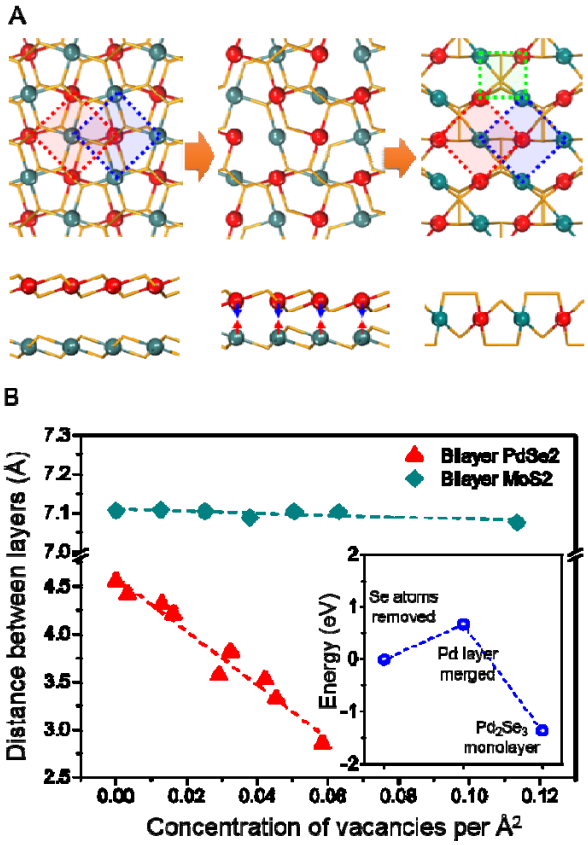

Figure 3: Interlayer fusion mechanism proposed by DFT calculations. (A) Schematic of the reconstruction mechanism from bilayer $PdSe_2$ to monolayer Pd_2Se_3. The red and blue dashed squares represent the square Pd networks from the two layers before merging, and the green one displays the newly fused Pd squared network in the same layer after merging. The Se atoms are not displayed. (B) Interlayer distance as a function of chalcogen vacancy concentration in bilayer $PdSe_2$ (red) and MoS_2 (green). In $PdSe_2$ the interlayer distance shows a clear decreasing trend as the vacancy concentration increased, while the change is negligible in MoS_2. Inset shows the energy landscape of each step of the interlayer fusion process.

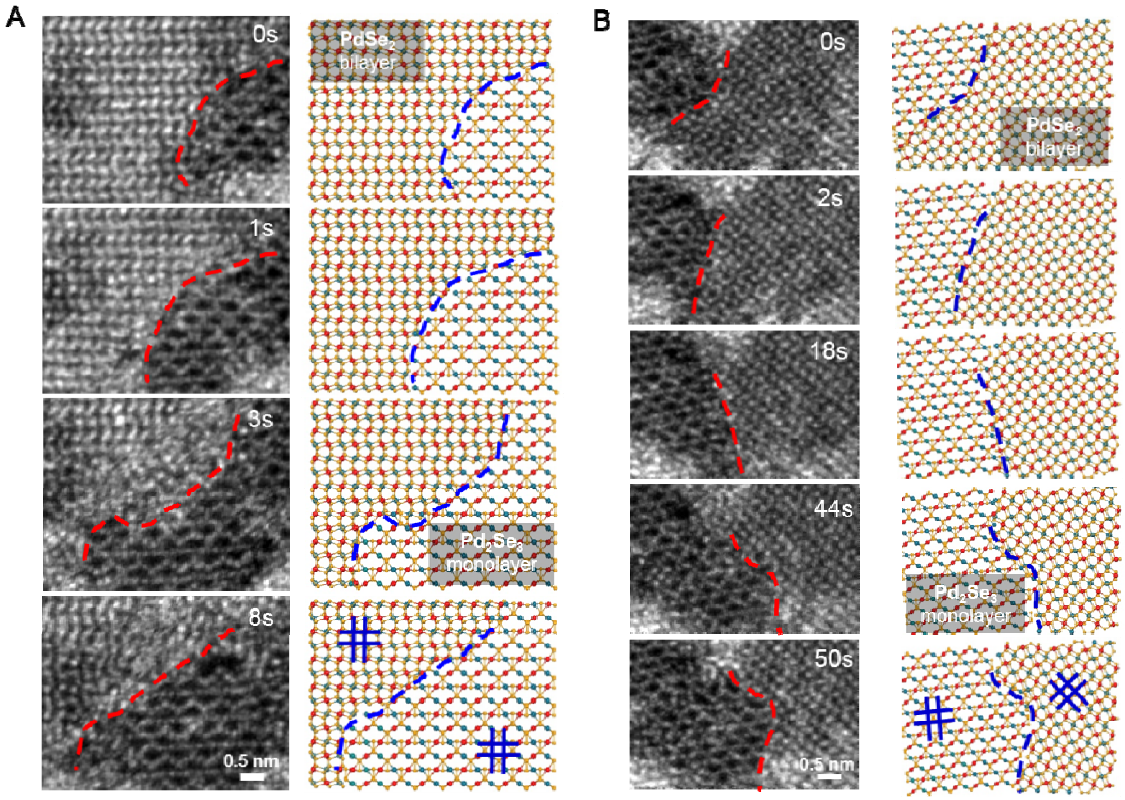

Figure 4: In-situ observation of the reconstruction process from $PdSe_2$ bilayer to Pd_2Se_3 monolayer. (A, B) Sequential ADF STEM images showing the examples of the growth of the monolayer Pd_2Se_3 extending to the few-layer $PdSe_2$ matrix as assisted by electron irradiation, with the same crystal orientation as the parent $PdSe_2$ (direct lattice fusion, A) and with a misorientation angle of ~37° (fusion and realign, B). The time scale is indicated in both sets of the images. The blue crossings indicate the orientation of the squared Pd network.